

Effects of the crystal structure on the ferromagnetic correlations in ZnO with magnetic impurities

Bo Gu¹, Nejat Bulut^{1,2}, and Sadamichi Maekawa^{1,2}

¹ *Institute for Materials Research, Tohoku University, Sendai 980-8577, Japan*

² *CREST, Japan Science and Technology Agency (JST), Kawaguchi, Saitama 332-0012, Japan*

We study the ferromagnetism in the compound (Zn,Mn)O within the Haldane-Anderson impurity model by using the quantum Monte Carlo technique and the tight-binding approximation for determining the host band-structure and the impurity-host hybridization. This computational approach allows us to determine how the host crystal structure influences the impurity bound state, which plays an important role in the development of the ferromagnetic (FM) correlations between the impurities. We find that the FM correlations are strongly influenced by the crystal structure. In particular, in p-type (Zn,Mn)O, we observe the development of FM correlations with an extended range at low temperatures for wurtzite and zincblende crystal structures. However, for the rocksalt structure no FM correlations are observed between the impurities. In addition, in n-type ZnO with magnetic impurities, the impurity bound state and FM correlations are not found.

PACS numbers: 75.50.Pp, 75.30.Hx, 75.40.Mg

I. INTRODUCTION

Dilute magnetic semiconductors (DMS) could lead to new spintronic devices where both the electronic charge and spin can be controlled. For practical applications, DMS with Curie temperature, T_c , above room temperature are required. The (Ga,Mn)As is regarded as a classic example with robust ferromagnetism [1], but the highest reported T_c 's are still well below room temperature [2, 3]. Alternatively, p-type (Zn,Mn)O has been predicted to be a room temperature ferromagnet [4, 5], where ferromagnetism above room temperature has been observed for Mn doped pure ZnO [6, 7, 8], or Mn doped p-type ZnO [9, 10, 11, 12, 13]. However, contradictory experimental results have also been reported for (Zn,Mn)O such as ferromagnetism below room temperature [14], absence of ferromagnetism [15], spin glass behavior [16], or paramagnetism [17].

The possibility of room-temperature ferromagnetism motivates the theoretical research on the origin and control of high-temperature ferromagnetism in semiconductors, especially ZnO-based DMS, which is the subject of this paper. Magnetic impurities in ordinary metals exhibit the well-known Ruderman-Kittel-Kasuya-Yosida (RKKY) oscillations, which is a carrier mediated indirect coupling due to the Friedel oscillations of the polarized carriers around the impurities. When magnetic impurities are doped into a semiconductor host, quite different behaviors are experimentally observed as mentioned above. The Haldane-Anderson impurity model had been introduced to study transition-metal impurities in semiconductors [18]. After the discovery of DMS, the magnetic properties of this model were addressed within the Hartree-Fock (HF) approximation [19], and it was shown that long-range ferromagnetic (FM) correlations develop when the Fermi level is located between the top of the valence band and the impurity bound state (IBS). The FM interaction between the impurities is mediated by

the impurity-induced polarization of the valence electron spins, which exhibit an antiferromagnetic coupling to the impurity moments. Subsequent Quantum Monte Carlo (QMC) calculations [20] on the two-impurity Haldane-Anderson model with the Hirsch-Fye algorithm have supported this picture for the generation of FM correlations between magnetic impurities in semiconductors. Various other theoretical approaches have also been used to study magnetic impurities in semiconductors. The Zener model has been invoked to describe the ferromagnetism in semiconductors [4]. Numerical calculations based on local spin density approximation (LSDA) have also found that magnetic states and corresponding Curie temperatures in ZnO-based DMS are controlled by changing the carrier density or the magnetic impurity concentration [5, 21, 22, 23, 24]. Within the context of DMS, the Anderson Hamiltonian for a semiconductor host was also considered by Krstajić *et al.* [25], and it was shown that an FM interaction is generated between the impurities due to kinematic exchange. The role of IBS in producing the FM interaction in DMS was also discussed within the “double resonance mechanism” using HF [26].

In this paper, we present QMC results for the compound (Zn,Mn)O. For ZnO host, the wurtzite structure is the most common phase, and thus almost all experiments for ZnO are focused on this structure. But ZnO with the zincblende and the rocksalt structures are also experimentally possible in thin films and at high pressure, respectively [27]. The band structures of ZnO with the wurtzite, zincblende and rocksalt structures had been already calculated within a single set of tight-binding parameters [27], and we will follow these results in this paper to study the ferromagnetism for the compound (Zn,Mn)O with experimentally determined values for the p - d mixing and the onsite Coulomb repulsion [28]. For the doped Mn²⁺ impurity, we neglect the Hund coupling among the five occupied $3d$ orbitals, and, for simplicity, consider the $3d$ orbitals independently. In the dilute impurity limit, the Haldane-Anderson impurity model is

invoked to describe the magnetic states of Mn^{2+} ions. The results of the numerical calculations show that the crystal structure of the ZnO host strongly influences the energy of the IBS and the strength of the magnetic correlations between the impurities. In particular, for the wurtzite and zincblende structures, we find that FM correlations with an extended range develop at low temperatures. However, for the rocksalt structure, FM correlations have not been observed, because, in this case, the IBS is located at much higher frequencies. In addition, only p-type (Zn,Mn)O is found to exhibit FM correlations.

In this paper, our purpose is to investigate the influence of the crystal structure of the semiconductor host on the FM correlations between the impurities. For this purpose, we combine the tight-binding calculations for the host band structure and the impurity-host hybridization with the QMC simulations. Our impurity model is simple, because we neglect the Hund couplings and consider only one of the $3d$ orbitals at the impurity site. However, this model is sufficient to demonstrate that the host crystal structure can be used to control ferromagnetism in DMS. Instead of the tight-binding approximation, the Local Density Approximations (LDA) can be used to calculate the host band structure and the impurity-host hybridization. In addition, it is possible to perform QMC simulations for all five of the impurity $3d$ orbitals with the Hund couplings. We think that this way of combining the LDA and QMC techniques can yield accurate predictions about ferromagnetism in DMS materials in the future.

II. IMPURITY MODEL

In order to describe the transition-metal impurities in a ZnO host, we use the Haldane-Anderson impurity model [18] which is defined by

$$\begin{aligned}
H = & \sum_{\mathbf{k},\alpha,\sigma} [\epsilon_{\alpha}(\mathbf{k}) - \mu] c_{\mathbf{k}\alpha\sigma}^{\dagger} c_{\mathbf{k}\alpha\sigma} \\
& + \sum_{\mathbf{k},\alpha,i,\xi,\sigma} (V_{i\xi\mathbf{k}\alpha} d_{i\xi\sigma}^{\dagger} c_{\mathbf{k}\alpha\sigma} + H.c.) \\
& + (E_d - \mu) \sum_{i,\xi,\sigma} d_{i\xi\sigma}^{\dagger} d_{i\xi\sigma} + U \sum_i n_{i\xi\uparrow}^{\dagger} n_{i\xi\downarrow}, \quad (1)
\end{aligned}$$

where $c_{\mathbf{k}\alpha\sigma}^{\dagger}$ ($c_{\mathbf{k}\alpha\sigma}$) is the creation (annihilation) operator for a host electron with wavevector \mathbf{k} and spin σ in the valence ($\alpha = v$) or conduction ($\alpha = c$) band, and $d_{i\xi\sigma}^{\dagger}$ ($d_{i\xi\sigma}$) is the creation (annihilation) operator for a localized electron at impurity site i in orbital ξ and spin σ with $n_{i\xi\sigma} = d_{i\xi\sigma}^{\dagger} d_{i\xi\sigma}$. Here, $\epsilon_{\alpha}(\mathbf{k})$ is the host band dispersion, μ the chemical potential, $V_{i\xi\mathbf{k}\alpha}$ the mixing between the impurity and host, E_d the impurity ξ -level energy, and U the onsite Coulomb repulsion for the impurity.

The energy bands $\epsilon_{\alpha}(\mathbf{k})$, and the impurity-host hybridization $V_{i\xi\mathbf{k}\alpha}$ will be calculated within the tight-

binding approximation for the wurtzite, zincblende and rocksalt crystal structures of the ZnO host material. For the compound (Zn,Mn)O, the value of the onsite Coulomb repulsion for Mn^{2+} is taken as $U = 5.2\text{eV}$ by comparing with the photoemission spectroscopy measurements [28]. In addition, because the experimental value of E_d for Mn^{2+} in ZnO host is unknown, in the following we use $E_d = \mu - U/2$ so that the impurity sites develop large magnetic moments. The results on the magnetic correlations between the impurities depend weakly on small variations on the value of E_d .

We note that, in Eq. (1), the Hund couplings among the different impurity $3d$ orbitals is neglected. In this paper, we consider only one of the $3d$ orbitals at the impurity site, since here our purpose is to demonstrate the effects of the host crystal structure on the FM correlations. Multi-orbital effects, where we keep all of the impurity $3d$ orbitals and the Hund couplings, will be studied with QMC in a separate paper.

III. TIGHT-BINDING APPROACH FOR THE ZnO BAND STRUCTURE AND THE IMPURITY-HOST HYBRIDIZATION

In this section, we discuss the tight-binding calculation of the band-structure of the ZnO host, and the impurity-host hybridization. The energy bands, $\epsilon_{\alpha}(\mathbf{k})$, of ZnO had been already calculated for the wurtzite, zincblende and rocksalt structures using a single set of sp^3 tight-binding parameters [27]. In this approach, the basis consists of one $4s$ and three $4p$ orbitals for cation Zn^{2+} and three $2p$ orbitals for anion O^{2-} . The values of the orbital energies are $E_p(\text{O}) = 0.550\text{ eV}$, $E_s(\text{Zn}) = 3.450\text{ eV}$, $E_p(\text{Zn}) = 13.050\text{ eV}$. In addition, the mixing values between the s , p orbitals of Zn^{2+} and the p orbitals of O^{2-} are taken to be $(sp\sigma) = 2.965\text{ eV}$, $(pp\sigma) = 4.324\text{ eV}$, and $(pp\pi) = -1.157\text{ eV}$.

Using these tight-binding parameters and keeping all of the branches within the sp^3 basis, we have reproduced the band structure of ZnO. In Figs. 1(a)-(c), we have plotted the branches near the semiconductor gap. Here, we observe that, for the wurtzite and zincblende structures, the top of the valence band is located at the Γ point with a direct gap of 3.45 eV. For the rocksalt case, the top of the valence band, located at the L point, is at 0.6 eV, while the Γ point is at -0.53 eV. Hence, for the rocksalt structure the system has an indirect semiconductor gap.

Next, we discuss the calculation of the impurity-host hybridization within the tight-binding approximation. Once a substitutional impurity Mn^{2+} is introduced and takes the position of a Zn^{2+} cation, the $3d$ orbital ξ of Mn^{2+} will mix with the neighboring $2p$ orbitals of O^{2-} . The mixing matrix element $V_{i\xi\mathbf{k}\alpha} \equiv \langle \varphi_{\xi}(\mathbf{i}) | H | \Psi_{\alpha}(\mathbf{k}) \rangle$ has

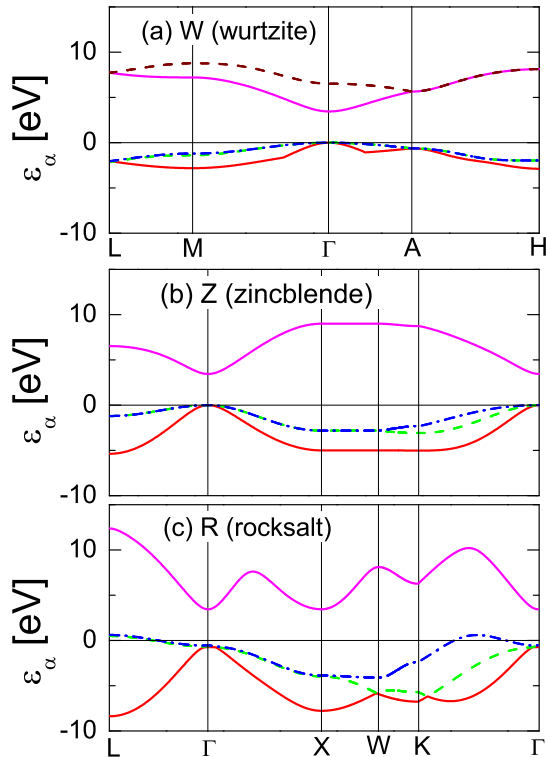


FIG. 1: Energy bands of the ZnO host near the semiconductor gap with (a) wurtzite, (b) zincblende, and (c) rocksalt crystal structures obtained using the tight-binding approximation. These results were reproduced using the parameters given in Ref. [27].

the form of

$$\begin{aligned}
 V_{i\xi\mathbf{k}\alpha} &= \frac{1}{\sqrt{N}} e^{i\mathbf{k}\cdot\mathbf{i}} \sum_{p,\mathbf{n}} e^{i\mathbf{k}\cdot(\mathbf{n}-\mathbf{i})} a_{\alpha p}(\mathbf{k}) \langle \varphi_{\xi}(\mathbf{i}) | H | \varphi_p(\mathbf{n}) \rangle \\
 &\equiv \frac{1}{\sqrt{N}} e^{i\mathbf{k}\cdot\mathbf{i}} V_{\xi\alpha}(\mathbf{k}),
 \end{aligned} \quad (2)$$

where $\varphi_{\xi}(\mathbf{i})$ is the impurity $3d$ -state at site \mathbf{i} , and $\Psi_{\alpha}(\mathbf{k})$ is the host state with wavevector \mathbf{k} and band index α , which is expanded by atomic orbitals $\varphi_p(\mathbf{n})$ with orbital index p and site index \mathbf{n} . Here, N is the total number of host lattice sites, and $a_{\alpha p}(\mathbf{k})$ is an expansion coefficient. For the p - d mixing integrals of $\langle \varphi_{\xi}(\mathbf{i}) | H | \varphi_p(\mathbf{n}) \rangle$, p represents the three $2p$ orbitals of O^{2-} , and ξ denotes the five $3d$ orbitals of Mn^{2+} . As shown by Slater and Koster [29], these fifteen mixing integrals can be expressed by only two integrals ($pd\sigma$) and ($pd\pi$) and direction cosines l , m and n in the two-center approximation. In this approach, the integrals ($pd\sigma$) and ($pd\pi$) are taken as fitting parameters which can then be determined by other exact results or by comparison with the experimental data. For the compound (Zn,Mn)O, the value of ($pd\sigma$) = -1.6 eV has been

estimated by comparing with the photoemission spectroscopy measurements [28], while the value of ($pd\pi$) is always determined by the relation ($pd\pi$) = $-(pd\sigma)/2.16$ [30]. We will use these values in the rest of this paper.

It is established that, for the wurtzite or zincblende crystal structures, the p - d mixing is dominated by the occupied t_{2g} (xy, yz, zx) orbitals because of the tetrahedral crystal field, while for the rocksalt structure, the p - d mixing comes mainly from the occupied e_g ($x^2 - y^2, z^2$) orbitals due to the octahedral crystal field [31]. In addition, the Hund coupling among the $3d$ orbitals of Mn^{2+} is neglected in this paper. In addition, for simplicity, here we consider only one of the t_{2g} orbitals ($\xi=xy$ orbital here) for the (Zn,Mn)O with wurtzite and zincblende structures, and only one of the e_g orbitals ($\xi = x^2 - y^2$ orbital here) for the (Zn,Mn)O with rocksalt structure. Hence, we treat the $3d$ orbitals of Mn^{2+} independently. In this paper, we are mainly interested in the effects of the host crystal structure, and we will treat the multi-orbital effects in a separate paper.

Figure 2 displays results on the the p - d mixing function $\overline{V}_{\xi}(\mathbf{k})$ defined by

$$\overline{V}_{\xi}(\mathbf{k}) \equiv \left(\sum_{\alpha} |V_{\xi\alpha}(\mathbf{k})|^2 \right)^{1/2} \quad (3)$$

where only one of the Mn^{2+} $3d$ orbitals, labeled by ξ , is considered. In Eq. (3), the summation over α is performed only over the valence bands (Fig. 2(a) and Fig. 2(c)) or the conduction bands (Fig. 2(b) and Fig. 2(d)). Here, $\overline{V}_{\xi}(\mathbf{k})$ is plotted along various cuts in the Brillouin zone for wurtzite, zincblende and rocksalt crystal structures. Figures 2(a) and (b) show \overline{V} for a Mn $3d(xy)$ orbital when the ZnO has the wurtzite structure. Here, we observe that, at the Γ point, the total hybridization of the xy orbital with the valence bands is about three times larger than that with the conduction bands. For the wurtzite and the zincblende structures, the semiconductor gap edges are located at the Γ point, hence the value of \overline{V} near Γ will be particularly important in determining the energy of the IBS and the strength of the magnetic correlations between the impurities. Figures 2(c) and (d) show that, for the case of a Mn $3d(xy)$ orbital in ZnO with the zincblende structure, the total hybridization with the valence bands is also stronger than that with the conduction bands near the Γ point. Figures 2(c) and (d) also show results for a Mn $3d(x^2 - y^2)$ orbital in the rocksalt structure. Here, we see that the total hybridization with the valence and the conduction bands vanish at the Γ point. However, at the L point, where the top of the valence band is located, the total hybridization with the valence band is the stronger than in the rest of the cases.

The results on the frequency of the IBS and the strength of the FM correlations depend sensitively on the value of hybridization near the gap edges, which we will discuss in the next section. We note that, in turn, the hybridization depends strongly on the values of the

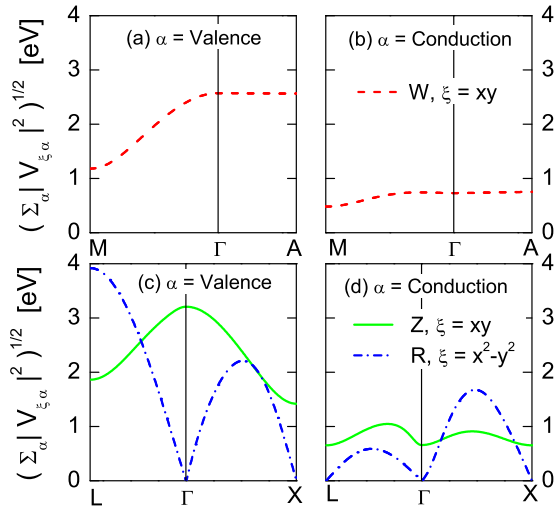


FIG. 2: Hybridization function $\bar{V}_\xi(\mathbf{k})$ of a single Mn^{2+} orbital with the valence bands ((a) and (c)) or the conduction bands ((b) and (d)). Here, results are shown for a Mn^{2+} $3d(xy)$ orbital in the wurtzite or zincblende ZnO and for a Mn^{2+} $3d(x^2 - y^2)$ orbital in the rocksalt ZnO. In obtaining these results, we have used mixing parameters with values taken from Ref. [28].

mixing parameters ($pd\sigma$) and ($pd\pi$) of the tight-binding approach.

IV. QUANTUM MONTE CARLO RESULTS

In this section, we present results on the impurity magnetic correlations, which were obtained using the Hirsch-Fye QMC technique [32]. The input parameters for the QMC simulations were calculated with the tight-binding approach described above. The following results were obtained with more than 10^5 Monte Carlo sweeps and Matsubara time step $\Delta\tau = 0.225$.

We first discuss the local moment formation at an impurity orbital. For this purpose, we have performed QMC simulations to calculate $\langle(M^z)^2\rangle$, where

$$M^z = n_{i\xi\uparrow} - n_{i\xi\downarrow} \quad (4)$$

is the magnetization operator for a single $3d(\xi)$ orbital at the impurity site \mathbf{i} . We have performed the calculations for a single $3d$ orbital because in this paper we are mainly interested in the effects of the host crystal and we neglect the multi-orbital effects, which we will treat in a separate paper. Hence, $\langle(M^z)^2\rangle$ represents the square of the local-moment for a single $3d$ orbital added to the ZnO host.

Figure 3(a) and (b) shows results on $\langle(M^z)^2\rangle$ for a $3d(xy)$ orbital in wurtzite and zincblende structures and a $3d(x^2 - y^2)$ orbital in the rocksalt ZnO. In Fig. 3(a),

$\langle(M^z)^2\rangle$ versus the chemical potential μ is plotted for $0 < \mu < 0.35\text{eV}$ and in Fig. 3(b) for $0 < \mu < 4\text{eV}$. These results are for temperature $T = 100\text{K}$. In these figures, we observe discontinuities at 0.12eV , 0.20eV and 1.6eV for the zincblende, wurtzite and rocksalt structures, respectively.

According to the Hartree-Fock and QMC calculations, the presence of a discontinuity in $\langle(M^z)^2\rangle$ versus μ implies the existence of an IBS at this energy [19, 20]. A step discontinuity develops in the magnitude of the magnetic moment as μ increases through ω_{IBS} , because impurity spectral weight is induced in the semiconductor gap at ω_{IBS} for sufficiently strong hybridization. When the IBS is occupied, the spin polarization of the host split-off state, which is due to the impurity-host mixing and at the same energy as the IBS, will cancel the spin polarization of the valence band. Thus antiferromagnetic couplings between the polarized host carriers and the impurities disappear. This causes the FM interaction between the impurities, which is mediated by the polarized carriers around the magnetic impurities, to vanish. In this paper, we are studying how this mechanism of ferromagnetic correlations is influenced by the crystal structure of the ZnO host. The variation in the values of ω_{IBS} for different crystal structures seen in Fig. 3 is clearly a consequence of the differences in the energy bands and the impurity-host mixing. In addition, the values of the hybridization with the bottom of the conduction bands are weaker, and hence we do not observe bound states near the bottom of the conduction band.

The value of ω_{IBS} plays an important role in determining the strength of the FM correlations which develop between the impurities when the IBS is unoccupied. Within the Hartree-Fock approximation and for a semiconductor host with constant density of states ρ_0 and semi-infinite bands [19], the range of the ferromagnetic (FM) correlations between the impurities is given by

$$\ell_0 \approx \frac{1}{\sqrt{16\pi\rho_0\omega_{IBS}}} \quad (5)$$

when the IBS is unoccupied ($0 < \mu < \omega_{IBS}$). However, when the IBS becomes occupied ($\omega_{IBS} < \mu$), the FM correlations become weaker. The QMC calculations performed for a two-dimensional (2D) semiconductor host with quadratic quasiparticle dispersion confirm this picture [20]. These QMC calculations show that, in 2D, ω_{IBS} increases as the strength of the hybridization grows. The maximum range of the FM correlations decreases as ω_{IBS} increases in agreement with the HF calculations. However, in the three-dimensional case, the IBS does not exist, if the hybridization is smaller than a critical value [33].

In the following calculations, we will see that the magnetic correlations between the impurities are sensitive to the location of the chemical potential with respect to the IBS. An IBS with shallower position ($\omega_{IBS}^Z \approx 0.1\text{eV}$) is obtained for (Zn,Mn)O with the zincblende structure,

while a much deeper IBS ($\omega_{IBS}^R \approx 1.6$ eV) is found for the rocksalt case. Based on the previous HF and QMC calculations [19, 20], it is reasonable to expect that the FM correlation range for (Zn,Mn)O with the wurtzite structure will be shorter than that with the zincblende structure, and will be much longer than that of the rocksalt case.

In addition, it should be pointed out that the IBS for (Zn,Mn)O with wurtzite and zincblende structures only exists near the top of valence band, while no IBS is found near the bottom of conduction band. If, instead of Mn^{2+} , another transition metal ion TM^{2+} is substituted into the ZnO host, then the only different quantities would be the p - d mixing parameters ($pd\sigma$) and ($pd\pi$) within this framework. In particular, for various hosts and transition-metal impurities, the p - d mixing parameters, which are consistent with the experimental measurements, are mostly in the range -1.6 eV \leq ($pd\sigma$) \leq -1.0 eV [28, 34], while ($pd\pi$) = $-(pd\sigma)/2.16$ [30]. We have checked the IBS for (Zn,TM)O for various p - d mixing values in the above mentioned range. We find that, when smaller values are used for the p - d mixing, the IBS shifts towards the top of valence band, while at the same time no IBS develops near the bottom of the conduction band. Since the doping of the transition metal ion TM^{2+} into the ZnO host does not itself introduce carriers, the hole and electron carriers in (Zn,TM)O are associated with *additional* the acceptor or donor defects, respectively. This implies that for p-type (Zn,TM)O, the FM correlations will develop when $0 \leq \mu \leq \omega_{IBS}$, while for the n-type (Zn,TM)O, no FM correlations are expected due to the absence of the IBS. In fact, the existence of p-type rather than n-type (Zn,Mn)O with wurtzite structure has recently been pointed out based on the analysis of the experimental measurements [12, 13].

We next display results on the impurity-impurity magnetic correlation function $\langle M_1^z M_2^z \rangle$ versus the impurity separation R/a in Fig. 4. These results are for two Mn^{2+} $3d$ orbitals, which are of the same type, added to the ZnO host. Clearly, in a more realistic calculation of FM correlations between the impurities, it would be necessary to consider the magnetic correlations between different types of $3d$ orbitals. However, our purpose in this paper is to investigate the role of the host electronic structure. In Fig. 4, the temperature $T = 200K$, $R = |R_1 - R_2|$, and a is the lattice constant. In our chosen directions, the distance between the 1st-nearest-neighboring Mn^{2+} is a for the wurtzite structure, while it is $a\sqrt{2}/2$ for the zincblende and rocksalt structures. As shown in Fig. 4(a) for the wurtzite structure, the impurity spins exhibit FM correlations at $\mu = 0.0$, but it is short range. By increasing μ to 0.15 eV, the range of the FM correlations becomes longer extending to the 3rd-nearest neighboring Mn^{2+} . Further increasing μ , the FM correlations becomes weaker. This is because the IBS of (Zn,Mn)O with wurtzite structure becomes occupied as μ changes above 0.15 eV, as seen in Fig. 3. For the zincblende structure, similar results are obtained as shown in Fig. 4(b): the

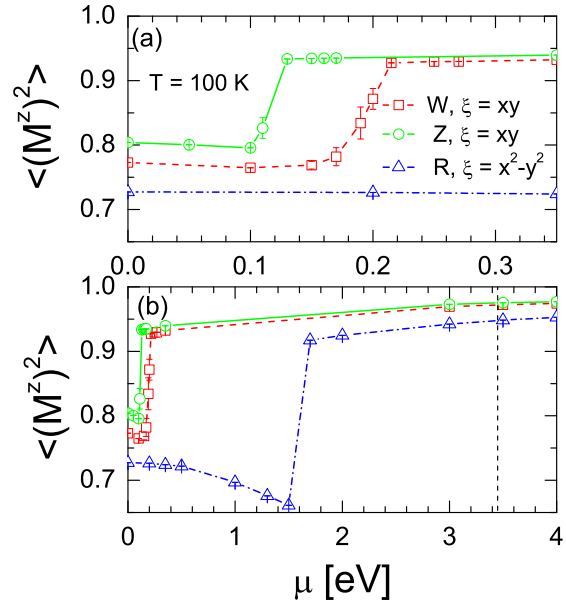


FIG. 3: Square of the magnetic moment at the impurity site, $\langle (M^z)^2 \rangle$, versus the chemical potential μ for different energy intervals at $T = 100K$. These results were obtained for a single Mn^{2+} $3d(\xi)$ orbital added to the ZnO host. For the wurtzite and zincblende crystal structures, we have considered a $\xi = xy$ orbital, while for the rocksalt case an $x^2 - y^2$ orbital. The vertical dashed line denotes the bottom of the conduction band.

impurity spins exhibit FM correlations extending to the 1st-nearest neighboring Mn^{2+} at $\mu = 0.0$. Increasing μ to 0.1 eV, the FM correlations extend to the 4th-nearest neighboring Mn^{2+} . Further increasing μ to above 0.1 eV, the FM correlations become weaker. This is because the IBS of (Zn,Mn)O with the zincblende structure becomes occupied as $\mu > 0.1$ eV, as displayed in Fig. 3. We note that the compound (Zn,Mn)O with the zincblende structure seems to possess a longer range for the FM correlations than that with the wurtzite structure, while almost all existing experiments for ZnO are focused on the wurtzite structure. Not surprisingly, we have not observed magnetic correlations for the rocksalt structure in Fig. 4(c). This is because the position of IBS for (Zn,Mn)O with rocksalt structure is too deep as seen in Fig. 3, thus the FM correlation range [19, 20] is shorter than the first nearest-neighbor distance.

We next study the temperature dependence of the ferromagnetic correlations between the impurities in different crystal structures. Figure 5 displays the T dependence of $\langle M_1^z M_2^z \rangle$ for impurities which are second-nearest neighbors in wurtzite, zincblende and rocksalt crystal structures. For wurtzite and zincblende structures, these calculations have been performed for the $3d(xy)$ orbitals, and for the rocksalt case they are for the $3d(x^2 - y^2)$ orbital. In addition, for the wurtzite and zincblende struc-

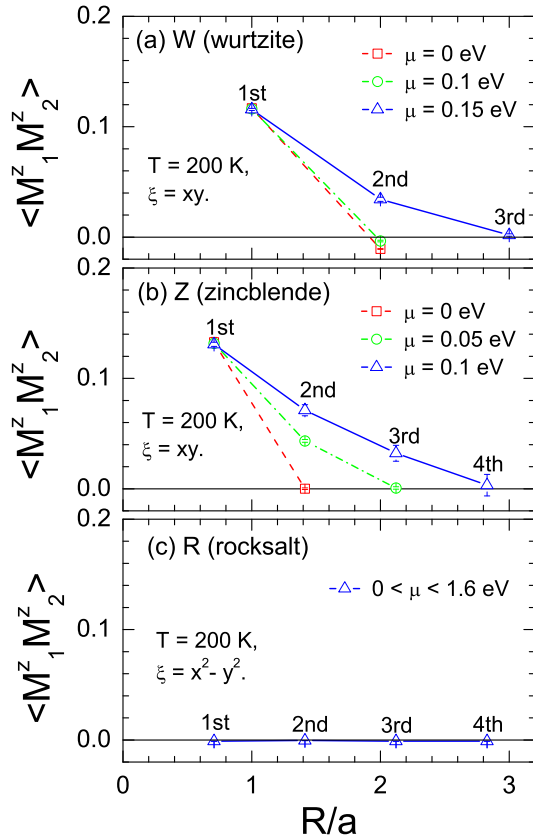


FIG. 4: Impurity-impurity magnetic correlation function $\langle M_1^z M_2^z \rangle$ versus distance R/a for (a) the wurtzite, (b) zincblende, and (c) rocksalt structures. Here, each impurity site consists of a single Mn^{2+} $3d$ orbital. For the wurtzite and zincblende crystal structure, we have considered a $3d(xy)$ orbital at the impurity sites, while for the rocksalt case a $3d(x^2 - y^2)$ orbital.

tures, the chemical potential is taken as $\mu = 0.15\text{ eV}$ and 0.1 eV , respectively, where the IBS is unoccupied and the longest range of the FM correlations occurs as shown in Fig. 4. The results for the rocksalt case are for $\mu = 1.5\text{ eV}$, so that the IBS is unoccupied here also. We observe that, as T decreases from 800 K down to 200 K , the FM correlations grow for the wurtzite and zincblende structures. In this T range, the FM do not develop for the rocksalt case.

V. DISCUSSION

For the ZnO host with the rocksalt structure, it is useful to mention previous studies [27, 35, 36] which are related to the *indirect* energy gaps obtained with the sp^3 tight-binding calculation shown in Fig. 1(c). Using the Hartree-Fock method, Jaffe et al. [35] pointed

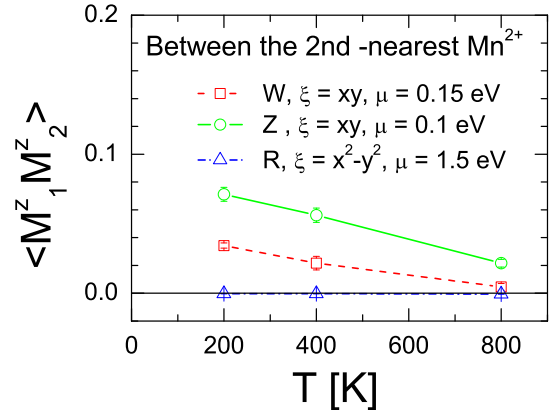


FIG. 5: Impurity-impurity magnetic correlation function $\langle M_1^z M_2^z \rangle$ for second nearest-neighbor impurity sites versus temperature T . Here, for the wurtzite and zincblende crystal structures, we have considered $3d(xy)$ orbitals, while for the rocksalt case $3d(x^2 - y^2)$ orbitals.

out that for the rocksalt ZnO, the point symmetry in rocksalt structure does not allow for mixing between the Zn $3d$ orbitals and the O $2p$ orbitals at the Γ point, but mixing is allowed elsewhere in the Brillouin zone. Thus the valence band maximum shifts away from the Γ point, so that the gap becomes *indirect*. As mentioned by Skinner and LaFemina in Ref.[27], where we follow their sp^3 tight-binding calculation for the ZnO host in present paper, this effect also exists even when the sp^3 tight-binding model does not *explicitly* include the Zn $3d$ orbitals, because the Zn $3d$ character has been *implicitly* included in the hopping integrals through the tight-binding interpolation of the bulk *ab initio* pseudopotential bands [36] that Skinner and LaFemina used to derive them.

However, there also exist calculations for the rocksalt ZnO, which are based on the quasiparticle approach [37] and the pseudopotential method [38], yielding a *direct* energy gap at the Γ point. In order to understand the results observed for (Zn,Mn)O with the rocksalt structure, we have considered the case of MgO, whose crystal structure is also rocksalt but has a *direct* energy gap at the Γ point [39]. Using the tight-binding parameters given in Ref. [39], where the host basis consists of one s orbital for Mg^{2+} and three $2p$ orbitals for O^{2-} , we have calculated the p - d mixing for the compound (Mg,Mn)O as in the case for (Zn,Mn)O. We found that, near the Γ point, the p - d mixing for (Mg,Mn)O with the rocksalt structure is also close to zero, where d stands for the five $3d$ orbitals. These results imply that the host compound with the rocksalt structure does not mix with the doped $3d$ orbitals at the Γ point regardless of whether there is a direct or indirect energy gap. In fact, this is generally true if the host with the rocksalt structure can be described using the sp^3 tight-binding approach. At the

Γ point, because of the orthogonality of the s and p orbitals, we find that, for a fixed band α , the coefficients $a_{\alpha p}$ in Eq.(2) have only one non-zero value, for example, a . Thus the p - d mixing at the Γ point has the form

$$V_{\alpha}(0) = a \sum_{\mathbf{n}} \langle \varphi_{\xi}(\mathbf{i}) | H | \varphi_p(\mathbf{n}) \rangle \equiv a \sum_{\mathbf{n}} E_{\xi,p}(\mathbf{i} - \mathbf{n}) \quad (6)$$

where ξ represents one of the five $3d$ orbitals, p denotes one of the s , p_x , p_y , and p_z orbitals. In addition, here, the summation is taken over the nearest neighbors, and $E_{\xi,p}(\mathbf{i} - \mathbf{n})$ is given using the notation of Slater and Koster [29], which can be expressed in terms of the non-zero ($pd\sigma$) and ($pd\pi$), and the direction cosines l , m , and n . For the rocksalt structure, it can be shown that the value of $V_{\alpha}(0)$, Eq. (6), vanishes for any ξ and p orbitals, when the summation is performed over the six nearest neighbors.

It is obvious that the magnetic correlations between the impurities depend on the position of the IBS, while the IBS is closely related the host band structure as well as the host-impurity mixing parameters. As mentioned above, for the rocksalt ZnO doped with magnetic impurities, the IBS will shift to the top of valence band if we decrease the values of the p - d mixing parameters ($pd\sigma$) and ($pd\pi$). Thus the detailed band structure calculations, such as LDA, are needed in the future to combine with QMC so that the ZnO-based DMS can be described more accurately.

VI. SUMMARY AND CONCLUSIONS

In summary, we have studied the ferromagnetism for the compound (Zn,Mn)O with different crystal structures in the dilute impurity limit based on the Haldane-Anderson impurity model. The band structures of the ZnO host were calculated using the sp^3 tight-binding parameters from Ref. [27], and the p - d mixing parameters and the onsite Coulomb repulsion U were obtained from comparisons with the photoemission measurements on (Zn,Mn)O [28]. The QMC calculations show that the magnetic correlations between Mn^{2+} impurities in ZnO are strongly affected by the host crystal structure. For the wurtzite and zinblende structures, the ferromagnetic

correlations are found, and their range extends up to the third or the fourth nearest neighbor sites at low temperatures. On the other hand, for the rocksalt structure, no magnetism has been found even between the nearest-neighbor impurities. In addition, only p-type ZnO doped with magnetic impurities is found to have ferromagnetism.

In this paper, our main purpose has been to investigate the effects of the crystal structure on the IBS and the FM correlations for the ZnO host. For simplicity, we have neglected the Hund coupling among the Mn^{2+} $3d$ orbitals. In addition, we have considered only one of the five $3d$ orbitals at the impurity sites. This is clearly an over simplification, however, it does allow us to demonstrate the role of the host crystal structure in determining the energy of the IBS and the maximum range of the FM correlations. Currently, we are in the process of performing QMC calculations which include all five of the $3d$ orbitals at the impurity site without neglecting the Hund couplings. In addition, we are using the LDA technique, instead of the tight-binding approximation, to calculate more precisely the host band structure and the impurity-host hybridization. We think that this LDA+QMC approach can be used to make accurate predictions about the FM correlations for different sets of DMS materials.

It is generally agreed up on that the ferromagnetism in the DMS can be controlled by changing the type of the transition-metal impurities or the host semiconductor as well as the occupation of the IBS. The results presented in this paper suggest that the host crystal structure can also be used in the search for high- T_c ferromagnetism in DMS.

ACKNOWLEDGMENTS

This work was supported by the NAREGI Nanoscience Project and a Grant-in Aid for Scientific Research from the Ministry of Education, Culture, Sports, Science and Technology of Japan, and NEDO. The authors thank the Supercomputer Center at the Institute for Solid State Physics, University of Tokyo, for the use of the facilities.

-
- [1] H. Ohno, A. Shen, F. Matsukura, A. Oiwa, A. Endo, S. Katsumoto, and Y. Iye, Appl. Phys. Lett. **69**, 363 (1996); H. Ohno, Science, **281**, 951 (1998).
 - [2] A. M. Nazmul, S. Sugahara, and M. Tanaka, Phys. Rev. B, **67**, 241308(R) (2003).
 - [3] T. Jungwirth, K. Y. Wang, J. Masek, K. W. Edmonds, J. Konig, J. Sinova, M. Polini, N. A. Goncharuk, A. H. MacDonald, M. Sawicki, A. W. Rushforth, R. P. Campion, L. X. Zhao, C. T. Foxon, and B. L. Gallagher, Phys. Rev. B **72**, 165204 (2005).
 - [4] T. Dietl, H. Ohno, F. Matsukura, J. Cibert, and D. Ferrand, Science, **287**, 1019 (2000).
 - [5] K. Sato, and H. K. Yoshida, Jpn. J. Appl. Phys. 40, L334 (2001); Physica E, **10**, 251 (2001).
 - [6] P. Sharma, A. Gupta, K. V. Rao, F. J. Owens, R. Sharma, R. Ahuja, J. M. O. Guillen, R. Johansson, and G. A. Gehring, Nat. Mater. **2**, 673 (2003).
 - [7] M. A. Garcia, M. L. Ruiz-Gonzalez, A. Quesada, J. L. Costa-Kramer, J. F. Fernandez, S. J. Khatib, A. Wennberg, A. C. Caballero, M. S. Martin-Gonzalez, M.

- Villegas, F. Briones, J. M. Gonzalez-Calbet, and A. Hernandez, Phys. Rev. Lett. **94**, 217206 (2005).
- [8] J. R. Neal, A. J. Behan, R. M. Ibrahim, H. J. Blythe, M. Ziese, A. M. Fox, and G. A. Gehring, Phys. Rev. Lett. **96**, 197208 (2006).
- [9] N. S. Norberg, K. R. Kittilstved, J. E. Amonette, R. K. Kukkadapu, D. A. Schwartz, and D. R. Gamelin, J. Am. Chem. Soc. **126**, 9387 (2004).
- [10] S. W. Lim, M. C. Jeong, M. H. Ham, and J. M. Myoung, Jpn. J. Appl. Phys. **43**, L280 (2004).
- [11] M. Ivill, S. J. Pearton, D. P. Norton, J. Kelly, and A. F. Hebard, J. Appl. Phys. **97**, 053904 (2005).
- [12] K. R. Kittilstved, N. S. Norberg, and D. R. Gamelin, Phys. Rev. Lett. **94**, 147209 (2005).
- [13] K. R. Kittilstved, W. K. Liu, and D. R. Gamelin, Nat. Mater. **5**, 291 (2006).
- [14] S. W. Jung, S. J. An, G. C. Yi, C. U. Jung, S. I. Lee, and S. Cho, Appl. Phys. Lett. **80**, 4561 (2002).
- [15] G. Lawes, A. S. Risbud, A. P. Ramirez, and R. Seshadri, Phys. Rev. B, **71**, 045201 (2005).
- [16] T. Fukumura, Z. Jin, M. Kawasaki, T. Shono, T. Hasegawa, S. Koshihara, and H. Koinuma, Appl. Phys. Lett. **78**, 958(2001).
- [17] A. Tiwari, C. Jin, A. Kvit, D. Kumar, J. F. Muth, J. Narayan, Solid State Commun. **121**, 371(2002).
- [18] F.D.M. Haldane and P.W. Anderson, Phys. Rev. B **13**, 2553 (1976).
- [19] M. Ichimura, K. Tanikawa, S. Takahashi, G. Baskaran, and S. Maekawa, *Foundations of Quantum Mechanics in the Light of New Technology*, eds. S. Ishioka and K. Fujikawa, (World Scientific, Singapore, 2006), 183-186, (cond-mat/0701736).
- [20] N. Bulut, K. Tanikawa, S. Takahashi, and S. Maekawa, Phys. Rev. B **76**, 045220 (2007).
- [21] K. Sato, and H. K. Yoshida, Phys. Stat. Sol. (b) **229**, 673 (2002).
- [22] H. K. Yoshida, and K. Sato, Physica B **327**, 337 (2003).
- [23] E. C. Lee, and K. J. Chang, Phys. Rev. B **69**, 085205 (2004).
- [24] N. A. Spaldin, Phys. Rev. B **69**, 125201 (2004).
- [25] P.M. Krstajić, V.A. Ivanov, F.M. Peeters, V. Fleurov, and K. Kikoin, Europhys. Lett. **61**, 235 (2003).
- [26] J. Inoue, S. Nonoyama, and H. Itoh, Phys. Rev. Lett. **85**, 4610 (2000).
- [27] A. J. Skinner and J. P. LaFemina, Phys. Rev. B **45**, 3557(1992).
- [28] T. Mizokawa, T. Nambu, A. Fujimori, T. Fukumura, and M. Kawasaki, Phys. Rev. B **65**, 085209 (2002).
- [29] J. C. Slater and G. F. Koster, Phys. Rev. **94**, 1498(1954).
- [30] *Electronic Structure and the Properties of Solids*, W. Harrison (Freeman, San Francisco, 1980)
- [31] *Physics of Transition Metal Oxides*, S. Maekawa, T. Tohyama, S. E. Barnes, S. Ishihara, W. Koshihara, and G. Khaliulin (Springer Series in Solid-State Sciences, Vol. 144, 2004)
- [32] J. E. Hirsch and R. M. Fye, Phys. Rev. Lett. **56**, 2521 (1986).
- [33] Y. Tomoda, N. Bulut, and S. Maekawa, unpublished.
- [34] J. W. Quilty, A. Shibata, J. Y. Son, K. Takubo, T. Mizokawa, H. Toyosaki, T. Fukumura, and M. Kawasaki, Phys. Rev. Lett. **96**, 027202 (2006).
- [35] J. E. Jaffe, R. Pandey, and A. B. Kunz, Phys. Rev. B **43**, 14030 (1991).
- [36] J. R. Chelikowsky, Solid State Commun. **22**, 351 (1977).
- [37] H. Q. Ni, Y. F. Lu, and Z. M. Ren, J. Appl. Phys. **91**, 1339 (2002).
- [38] D. Fritsch, H. Schmidt, and M. Grundmann, Appl. Phys. Lett. **88**, 134104 (2006).
- [39] V. C. Lee, and H. S. Wong, J. Phys. Soc. Jpn. **45**, 895 (1978).